Multiple Pulse Excitation of Molecular Vibration in Resonant Pump-Probe Experiments. I. Perturbative Approach

Hitoshi KAWASHIMA and Tadamasa SHIDA*
Department of Chemistry, Faculty of Science, Kyoto University, Kyoto 606-01
(Received January 11, 1993)

The possibility of stepwise amplification of molecular vibration by resonant multiple pulse excitation is theoretically considered on the basis of perturbation theory. A grating experiment favorable to its observation is proposed. It has proved that the effective interval of the repetitive irradiation to attain large amplitude vibrations is equal to odd halves of the period of the vibrational cycle and that there is no gain with an interval equal to the integral multiples of the vibrational period while such an interval is effective in mode selective excitation. It has also proved that the dispersed signal shifts periodically over a range of energy and that the range is widened as the vibrational amplitude is increased.

The pump-probe techniques have attracted interest since it facilitates the real time observation of ultrafast dynamics in condensed phases. In its application to vibrational spectroscopy, the material system is subjected to a ultrashort perturbation by pump pulses to be distorted abruptly along an active mode from the equilibrium structure, and the time evolution of the system is monitored by the variably delayed probe pulse. The nonstationary state initially prepared, therefore, determines the dynamics in spectroscopic manifestation. The mechanisms to drive an active mode to displace differ according to whether the optical pulse is resonant with the electronic transition or not; in the off-resonance case, the driving force from the pump field is exerted through the polarizability derivative, and the initial displacement can be made larger by the more intense pulse. In the resonant case, by contrast, the role of the pump pulse is just to switch the two relevant potential surfaces upon which the wavepacket should move. Therefore, it might appear that the initial displacement cannot be controlled by the strength of the external field. However, larger displacements can be achieved by multiple pulse excitation; recently, Weiner et al. have conducted an impulsive stimulated Raman scattering experiment using specially devised femtosecond pulse trains and have demonstrated enhanced scattering from a selected active mode.[1] Gerdy et al. have reported building up of the wavepacket population by resonant multiple excitation.[2] The population discussed by them is of the second order in the pump field and not the higher order as treated here. In the present paper we will propose the resonant multiple excitation resulting in a large amplitude vibrational motion that extends beyond the Franck–Condon region. In particular, it will be predicted how the large amplitude motion appears in the spectral and temporal signals.

Theoretical

Spatial Coupling and Nonlinear Polarization. The resonant medium considered here is an electronically two-level system which is coupled to molecular vibrations as is exemplified by dye molecules in solution. For the arguments which follow, Assumptions 1)—6) will be made; 1) the slowly varying amplitude approximation is applicable. 2) the Condon approximation is valid. 3) the relaxation of nuclear motion is negligible. 4) the time intervals between the successive pairs of pumping pulses, and between the last pumping pair and the probe pulse are much longer than the homogeneous transverse relaxation time T_2. Accordingly, the electronic coherence induced by any one pulse decays out completely before the arrival of the next pulse. 5) the optical pulses are weak enough to assure the validity of the perturbative treatment. 6) the temporal width of every optical pulse is so short that dynamics of the system such as the optical dephasing and molecular vibrations is regarded as frozen during an irradiation.

We have in mind a kind of transient grating experiments which will be outlined as follows; a definite number of pulse pairs on different arms are successively sent into the sample with a certain interval of time between the neighboring pair. The two pulses in each pair are temporally and spatially overlaps inside the sample to induce the spatially modulated population inversion, i.e., the population grating. After the transmission of all the pairs, a probe pulse denoted as E_p is incident on the material and is diffracted by the grating into various directions. The diffraction into a particular direction is detected as is illustrated in Fig. 1a.

Suppose the simplest case of the excitation by a single pair of pump pulses, say E_1 and E_2 and attempt to detect the diffraction along the direction parallel to $\vec{n}_p \pm (\vec{n}_1 - \vec{n}_2)$, where $\vec{n}_p$, $\vec{n}_1$, and $\vec{n}_2$ represent the unit vectors along the propagation directions of the probe pulse E_p, the pump pulses E_1 and E_2, respectively. We shall consider another excitation mode, i.e., exciting the sample with the succeeding pair of pulses E_3 (along $\vec{n}_3$) and E_4 (along $\vec{n}_4$), and attempt the detection of the diffracted light into $\vec{n}_p \pm (\vec{n}_1 - \vec{n}_2) \pm (\vec{n}_3 - \vec{n}_4)$. We further consider the mode involving the additional pair of pluses E_5 (along $\vec{n}_5$) and E_6 (along $\vec{n}_6$) and will be concerned about the diffraction into $\vec{n}_p \pm (\vec{n}_1 - \vec{n}_2) \pm (\vec{n}_3 -$

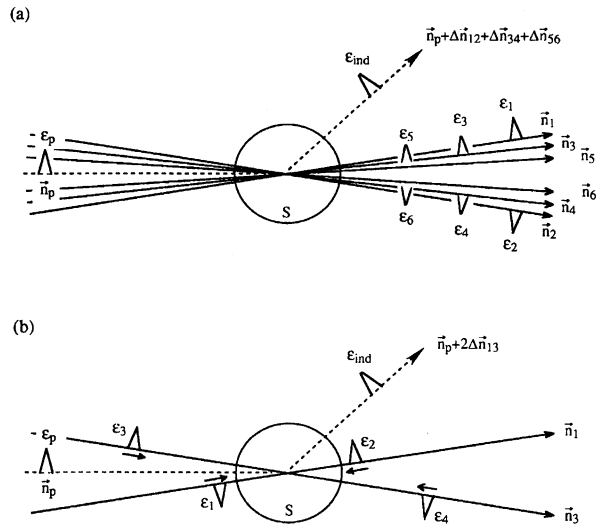

Fig. 1. Schematic representation of the experimental arrangement. Panel (a) corresponds to the triple excitation case, where S represents the sample and $\Delta\vec{n}_{ij}\equiv\vec{n}_i-\vec{n}_j$. The intersecting angles between $\vec{n}_1$ and $\vec{n}_2$, $\vec{n}_3$ and $\vec{n}_4$, and $\vec{n}_5$ and $\vec{n}_6$ should be taken as small as possible in a real experiment. Panel (b) depicts an alternative arrangement for the double excitation case.

$\vec{n}_4)\pm(\vec{n}_5-\vec{n}_6)$. For the last case involving three pairs of excitation pulses, an example of the beam-geometry is shown in Fig. 1a. The implication of Fig. 1a will be explained later in the section of Significance of Grating Arrangement.

The diffraction intensity varies for different combinations of the signs in coupling the wave vectors because there exists a partial breakdown in the phase-matching condition caused by discrepancy of the lengths of those vectors from unity. Except for such difference in the absolute intensities, all the combinations give a common signal of beating, which will be described later in detail.

As a representative case, the explicit form of the nonlinear polarization associated with the excitation by three pairs of pulses will be given. The electric field of an optical pulse E_i (i=1, 2, ⋯, or p) is assumed to take the form as

$$E_i(t,\vec{r}) = \varepsilon_i(t-(\vec{n}_i\cdot\vec{r})/c)\,e^{i\omega_1(t-(\vec{n}_i\cdot\vec{r})/c)} + \text{c.c.}, \qquad (1)$$

where c denotes the velocity of light, and ε_i(t) represents the temporal envelope that varies slowly compared with its carrier frequency ω_1. From now on an individual pulse is identified by the notation of its envelope for convenience. In the triple excitation in Fig. 1a, the source of the detected scattering is the seventh order polarization in the form

$$P^{(7)}(t,\vec{r}) = \hat{P}^{(7)}(t,\vec{r})\,e^{i\omega_1 t} + \text{c.c.}, \qquad (2)$$

where $\hat{P}^{(7)}$(t,$\vec{r}$) expresses a temporal envelope. Solving the Liouville equation perturbatively under Assumptions 1—6, we obtain the polarization envelope

$$\begin{aligned}
\hat{P}^{(7)}(t,\vec{r}) = (-i)^7\mathcal{N}|p_{ge}|^8 &\int_0^{t-(\vec{n}_g\cdot\vec{r})/c} dt_7 \int_0^{t_7+(\Delta\vec{n}_{gf}\cdot\vec{r})/c} dt_6 \int_0^{t_6+(\Delta\vec{n}_{fe}\cdot\vec{r})/c} dt_5 \\
&\int_0^{t_5+(\Delta\vec{n}_{ed}\cdot\vec{r})/c} dt_4 \int_0^{t_4+(\Delta\vec{n}_{dc}\cdot\vec{r})/c} dt_3 \\
&\int_0^{t_3+(\Delta\vec{n}_{cb}\cdot\vec{r})/c} dt_2 \int_0^{t_2+(\Delta\vec{n}_{ba}\cdot\vec{r})/c} dt_1 \\
&\{\varepsilon_g(t_7)\varepsilon_f^*(t_6)\varepsilon_e(t_5)\varepsilon_d^*(t_4)\varepsilon_c(t_3)\varepsilon_b^*(t_2)\varepsilon_a(t_1) \\
&e^{-i(\omega_1/c)\vec{n}_{s1}\cdot\vec{r}}R_1^{(7)}(t-t_7,t_7-t_6,t_6-t_5,t_5-t_4, \\
&t_4-t_3,t_3-t_2,t_2-t_1) \\
&+\varepsilon_g(t_7)\varepsilon_f^*(t_6)\varepsilon_e(t_5)\varepsilon_d^*(t_4)\varepsilon_c(t_3)\varepsilon_b(t_2)\varepsilon_a^*(t_1) \\
&e^{-i(\omega_1/c)\vec{n}_{s2}\cdot\vec{r}}R_2^{(7)}(t-t_7,t_7-t_6,t_6-6_5,t_5-t_4, \\
&t_4-t_3,t_3-t_2,t_2-t_1) \\
&+\varepsilon_g(t_7)\varepsilon_f^*(t_6)\varepsilon_e(t_5)\varepsilon_d(t_4)\varepsilon_c^*(t_3)\varepsilon_b(t_2)\varepsilon_a^*(t_1) \\
&e^{-i(\omega_1/c)\vec{n}_{s3}\cdot\vec{r}}R_3^{(7)}(t-t_7,t_7-t_6,t_6-6_5,t_5-t_4, \\
&t_4-t_3,t_3-t_2,t_2-t_1) \\
&+\varepsilon_g(t_7)\varepsilon_f^*(t_6)\varepsilon_e(t_5)\varepsilon_d(t_4)\varepsilon_c^*(t_3)\varepsilon_b^*(t_2)\varepsilon_a(t_1) \\
&e^{-i(\omega_1/c)\vec{n}_{s4}\cdot\vec{r}}R_4^{(7)}(t-t_7,t_7-t_6,t_6-6_5,t_5-t_4, \\
&t_4-t_3,t_3-t_2,t_2-t_1) \\
&+\varepsilon_g(t_7)\varepsilon_f(t_6)\varepsilon_e^*(t_5)\varepsilon_d(t_4)\varepsilon_c^*(t_3)\varepsilon_b(t_2)\varepsilon_a^*(t_1) \\
&e^{-i(\omega_1/c)\vec{n}_{s5}\cdot\vec{r}}R_5^{(7)}(t-t_7,t_7-t_6,t_6-6_5,t_5-t_4, \\
&t_4-t_3,t_3-t_2,t_2-t_1) \\
&+\varepsilon_g(t_7)\varepsilon_f(t_6)\varepsilon_e^*(t_5)\varepsilon_d(t_4)\varepsilon_c^*(t_3)\varepsilon_b^*(t_2)\varepsilon_a(t_1) \\
&e^{-i(\omega_1/c)\vec{n}_{s6}\cdot\vec{r}}R_6^{(7)}(t-t_7,t_7-t_6,t_6-6_5,t_5-t_4, \\
&t_4-t_3,t_3-t_2,t_2-t_1) \\
&+\varepsilon_g(t_7)\varepsilon_f(t_6)\varepsilon_e^*(t_5)\varepsilon_d^*(t_4)\varepsilon_c(t_3)\varepsilon_b^*(t_2)\varepsilon_a(t_1) \\
&e^{-i(\omega_1/c)\vec{n}_{s7}\cdot\vec{r}}R_7^{(7)}(t-t_7,t_7-t_6,t_6-6_5,t_5-t_4, \\
&t_4-t_3,t_3-t_2,t_2-t_1) \\
&+\varepsilon_g(t_7)\varepsilon_f(t_6)\varepsilon_e^*(t_5)\varepsilon_d^*(t_4)\varepsilon_c(t_3)\varepsilon_b(t_2)\varepsilon_a^*(t_1) \\
&e^{-i(\omega_1/c)\vec{n}_{s8}\cdot\vec{r}}R_8^{(7)}(t-t_7,t_7-t_6,t_6-6_5,t_5-t_4, \\
&t_4-t_3,t_3-t_2,t_2-t_1)\}, \qquad (3)
\end{aligned}$$

where $\mathcal{N}$ and p_{ge} denote the number density of the absorbers and the transition dipole, respectively. The difference vectors are defined as $\Delta\vec{n}_{ij}\equiv\vec{n}_i-\vec{n}_j$, and $\varepsilon_a(t)$, $\varepsilon_b(t)$, ⋯, and $\varepsilon_g(t)$ correspond to $\varepsilon_1(t)$, $\varepsilon_2(t)$, ⋯, $\varepsilon_6(t)$, or $\varepsilon_p(t)$. Here, we do not write down the explicit forms of the seventh order response functions $R_i^{(7)}(t-t_7, \cdots, t_2-t_1)$ (i=1—8) since it is not their complete but reduced forms that is required after all as will be shown later. The eight terms in Eq. 3 possess the respective phase factors involving the propagation directions $\vec{n}_{si}$ (i=1—8) which are given by

$$\vec{n}_{s1} \equiv \vec{n}_g - \vec{n}_f + \vec{n}_e - \vec{n}_d + \vec{n}_c - \vec{n}_b + \vec{n}_a,$$
$$\vec{n}_{s2} \equiv \vec{n}_g - \vec{n}_f + \vec{n}_e - \vec{n}_d + \vec{n}_c + \vec{n}_b - \vec{n}_a,$$

$$\vec{n}_{s3} \equiv \vec{n}_g - \vec{n}_f + \vec{n}_e + \vec{n}_d - \vec{n}_c + \vec{n}_b - \vec{n}_a,$$
$$\vec{n}_{s4} \equiv \vec{n}_g - \vec{n}_f + \vec{n}_e + \vec{n}_d - \vec{n}_c - \vec{n}_b + \vec{n}_a,$$
$$\vec{n}_{s5} \equiv \vec{n}_g + \vec{n}_f - \vec{n}_e + \vec{n}_d - \vec{n}_c + \vec{n}_b - \vec{n}_a,$$
$$\vec{n}_{s6} \equiv \vec{n}_g + \vec{n}_f - \vec{n}_e + \vec{n}_d - \vec{n}_c - \vec{n}_b + \vec{n}_a,$$
$$\vec{n}_{s7} \equiv \vec{n}_g + \vec{n}_f - \vec{n}_e - \vec{n}_d + \vec{n}_c - \vec{n}_b + \vec{n}_a,$$
and $$\vec{n}_{s8} \equiv \vec{n}_g + \vec{n}_f - \vec{n}_e - \vec{n}_d + \vec{n}_c + \vec{n}_b - \vec{n}_a.$$

The radiation into $\vec{n}_p+(\vec{n}_1-\vec{n}_2)+(\vec{n}_3-\vec{n}_4)+(\vec{n}_5-\vec{n}_6)$ arises from a particular assignment of the fields in the eight terms in Eq. 3. The definite assignment is listed in Table 1a. It is obvious that the eight propagation vectors $\vec{n}_{s1}$ through $\vec{n}_{s8}$ are all equivalent. Henceforth, we omit the spatially dependent phase factor which is common to all the eight terms, and denote the polarization in Eq. 3 simply as $\hat{P}^{(7)}(t)$. We set the interval of time between the first and the second pairs of coincident pulses to be τ_1, the one between the second and the third pairs be τ_2, and the last one between the third and the probe pulse be τ. Suppose that the first pair of coincident pulses are incident on the sample at $t=0$. The pulse envelopes can be replaced with δ functions by Assumption 6, and written as

Table 1. Field Assignment

(a)

	ε_g	ε_f	ε_e	ε_d	ε_c	ε_b	ε_a
1	ε_p	ε_6	ε_5	ε_4	ε_3	ε_2	ε_1
2	ε_p	ε_6	ε_5	ε_4	ε_3	ε_1	ε_2
3	ε_p	ε_6	ε_5	ε_3	ε_4	ε_1	ε_2
4	ε_p	ε_6	ε_5	ε_3	ε_4	ε_2	ε_1
5	ε_p	ε_5	ε_6	ε_3	ε_4	ε_1	ε_2
6	ε_p	ε_5	ε_6	ε_3	ε_4	ε_2	ε_1
7	ε_p	ε_5	ε_6	ε_4	ε_3	ε_2	ε_1
8	ε_p	ε_5	ε_6	ε_4	ε_3	ε_1	ε_2

(b)

	ε_c	ε_c	ε_a
1	ε_p	ε_2	ε_1
2	ε_p	ε_1	ε_2

(c)

	ε_e	ε_d	ε_c	ε_b	ε_a
1	ε_p	ε_4	ε_3	ε_2	ε_1
2	ε_p	ε_4	ε_3	ε_1	ε_2
3	ε_p	ε_3	ε_4	ε_1	ε_2
4	ε_p	ε_3	ε_4	ε_1	ε_2

(a) For the seventh order polarization propagating along $\vec{n}_p+(\vec{n}_1-\vec{n}_2)+(\vec{n}_3-\vec{n}_4)+(\vec{n}_5-\vec{n}_6)$, (b) For the third order polarization propagating along $\vec{n}_p+(\vec{n}_1-\vec{n}_2)$, and (c) For the fifth order polarization propagating along $\vec{n}_p+(\vec{n}_1-\vec{n}_2)+(\vec{n}_3-\vec{n}_4)$. The columns in (a) correspond to the fields ε_g through ε_a in Eq. 3, and the running numbers of the rows correspond to those of the response functions in Eq. 3. Similarly, the two rows in (b) and the four in (c) correspond to the two response functions of the third order and the four response functions of the fifth order, respectively.

$$\varepsilon_1(t) = \varepsilon_2(t) = \varepsilon_1\tau_p\delta(t),$$
$$\varepsilon_3(t) = \varepsilon_4(t) = \varepsilon_3\tau_p\delta(t-\tau_1)\,e^{-i\omega_1\tau_1},$$
$$\varepsilon_5(t) = \varepsilon_6(t) = \varepsilon_5\tau_p\delta(t-\tau_2-\tau_1)\,e^{-i\omega_1(\tau_2+\tau_1)},$$
and $$\varepsilon_p(t) = \varepsilon_p\tau_p\delta(t-\tau-\tau_2-\tau_1)\,e^{-i\omega_1(\tau+\tau_2+\tau_1)}, \quad (4)$$

where τ_p is the temporal width of the optical pulses. Referring to Table 1a, we substitute Eq. 4 into Eq. 3, and neglect the spatial dependence in the upper limits of the integral for simplicity while integrating over t_1 through t_7. All the eight terms result in the following form

$$(1/8)(-i)^7\mathcal{N}\theta_1{}^2\theta_3{}^2\theta_5{}^2\theta_p p_{ge} R_i^{(7)}(t-\tau-\tau_2-\tau_1,\tau,0,\tau_2,0,\tau_1,0), \quad (5)$$

where $\theta_i \equiv p_{ge}\varepsilon_i\tau_p$ ($i=1$, 3, 5 and p) with $\theta_i \ll 1$ by Assumption 5. The factor 1/8 comes from the fact that three half-delta functions are involved in the sevenfold integration. Since the following relation holds generally

$$R_1^{(7)}(s_7,s_6,0,s_4,0,s_2,0) = R_2^{(7)}(s_7,s_6,0,s_4,0,s_2,0) = \cdots = R_8^{(7)}(s_7,s_6,0,s_4,0,s_2,0), \quad (6)$$

the eight terms in Eq. 3 are in a common form to give the seventh order polarization

$$\hat{P}^{(7)}(t) = (-i)^7\mathcal{N}\theta_1{}^2\theta_3{}^2\theta_5{}^2\theta_p p_{ge} R^{(7)}(t-\tau-\tau_2-\tau_1,\tau,\tau_2,\tau_1) \quad \text{for } t > \tau_1+\tau_2+\tau, \quad (7)$$

where $R^{(7)}(s_7, s_6, s_4, s_2)$ is defined as in Eq. 6.

If the material is excited by only a single pair of pulses, the two coincident pulses are assumed to be incident on the sample at $t=0$, and the probe pulse is at $t=\tau$. Likewise, in the double excitation mode the first and the second pairs of coincident pulses are assumed to be incident at $t=0$ and $t=\tau_1$, respectively, and the probe pulse is delayed from the second pair by an interval of τ. The scattering to be detected in the single excitation mode arises from the third order polarization whereas in the double excitation mode from the fifth order polarization. The former incorporates two response functions, $R_i^{(3)}(s_3, s_2, s_1)$ ($i=1$ and 2), and the latter four, $R_i^{(5)}(s_5, s_4, s_3, s_2, s_1)$ ($i=1$—4), the explicit forms of which are not given here. The components propagating along $\vec{n}_p+(\vec{n}_1-\vec{n}_2)$ and along $\vec{n}_p+(\vec{n}_1-\vec{n}_2)+(\vec{n}_3-\vec{n}_4)$ follow the assignments given in Tables 1b and 1c, respectively. With a procedure similar to that in the triple excitation mode, one can obtain the relevant polarizations as follows by introducing $R^{(3)}(s_3,s_2) \equiv R_i^{(3)}(s_3,s_2,0)$ ($i=1$ or 2) and $R^{(5)}(s_5,s_4,s_2) \equiv R_i^{(5)}(s_5,s_4,0,s_2,0)$ ($i=1, 2, \cdots$, or 4).

$$\hat{P}^{(3)}(t) = (-i)^3\mathcal{N}\theta_1{}^2\theta_p p_{ge} R^{(3)}(t-\tau,\tau) \quad \text{for } t > \tau \quad (8)$$

and

$$\hat{P}^{(5)}(t) = (-i)^5 \mathcal{N}\theta_1{}^2\theta_3{}^2\theta_{\mathrm{p}}p_{\mathrm{ge}}R^{(5)}(t-\tau-\tau_1,\tau,\tau_1) \quad \text{for } t > \tau_1+\tau. \tag{9}$$

The reduced response functions in Eqs. 7, 8, and 9 are expressed as follows in terms of the constituent functions defined by Eqs. 13a, 13b, 13c, and 13d

$$R^{(3)}(s,\tau) = \mathrm{e}^{-\tau/T_1}\{v_0 + v_1(\tau)\}, \tag{10}$$

$$R^{(5)}(s,\tau,\tau_1) = \mathrm{e}^{-(\tau+\tau_1)/T_1} \times \{v_0 + v_1(\tau) + v_1(\tau+\tau_1) + v_2(\tau;\tau_1)\}, \tag{11}$$

and

$$R^{(7)}(s,\tau,\tau_2,\tau_1) = \mathrm{e}^{-(\tau+\tau_2+\tau_1)/T_1} \times \{v_0 + v_1(\tau) + v_1(\tau+\tau_2) + v_1(\tau+\tau_2+\tau_1) + v_2(\tau+\tau_2;\tau_1) + v_2(\tau;\tau_2) + v_2(\tau;\tau_2+\tau_1) + v_3(\tau;\tau_2,\tau_1)\}. \tag{12}$$

The constituent response functions are defined by

$$v_0 \equiv \mathrm{e}^{i\Delta_0 s}\mathrm{e}^{-\sigma^2 s^2}\mathrm{e}^{-s/T_2}\langle\phi_0\left|U_{\mathrm{e}}^{\dagger}(s)U_{\mathrm{g}}(s)\right|\phi_0\rangle, \tag{13a}$$

$$v_1(\tau) \equiv \mathrm{e}^{i\Delta_0 s}\mathrm{e}^{-\sigma^2 s^2}\mathrm{e}^{-s/T_2}\langle\phi_0\left|U_{\mathrm{e}}^{\dagger}(\tau+s)U_{\mathrm{g}}(s)U_{\mathrm{e}}(\tau)\right|\phi_0\rangle, \tag{13b}$$

$$v_2(\tau;\tau_1) \equiv \mathrm{e}^{i\Delta_0 s}\mathrm{e}^{-\sigma^2 s^2}\mathrm{e}^{-s/T_2} \times\langle\phi_0\left|U_{\mathrm{e}}^{\dagger}(\tau_1)U_{\mathrm{g}}^{\dagger}(\tau)U_{\mathrm{e}}^{\dagger}(s)U_{\mathrm{g}}(s+\tau)U_{\mathrm{e}}(\tau_1)\right|\phi_0\rangle, \tag{13c}$$

and

$$v_3(\tau;\tau_2,\tau_1) \equiv \mathrm{e}^{i\Delta_0 s}\mathrm{e}^{-\sigma^2 s^2}\mathrm{e}^{-s/T_2}\langle\phi_0\left|U_{\mathrm{e}}^{\dagger}(\tau_1)U_{\mathrm{g}}^{\dagger}(\tau_2)U_{\mathrm{e}}^{\dagger}(\tau+s)\right. \left.U_{\mathrm{g}}(s)U_{\mathrm{e}}(\tau)U_{\mathrm{g}}(\tau_2)U_{\mathrm{e}}(\tau_1)\right|\phi_0\rangle \tag{13d}$$

with

$$U_{\mathrm{g}}(s) \equiv \mathrm{e}^{-iH_{\mathrm{g}}s} \quad \text{and} \quad U_{\mathrm{e}}(s) \equiv \mathrm{e}^{-iH_{\mathrm{e}}s}. \tag{14}$$

Here, Δ_0 is a detuning frequency of the purely electronic transition from that of the incident radiation, σ is a measure of inhomogeneous broadening for the electronic transition, T_2 and T_1 are characteristic decay constants for the electronic coherence and population inversion, respectively. The symbol $|\phi_0\rangle$ denotes the zero-vibrational state in the electronic ground state, and $U_{\mathrm{g}}(s)$ and $U_{\mathrm{e}}(s)$ are nuclear propagators during an interval of s under the vibrational Hamiltonians H_{g} and H_{e} in the electronic ground and excited states, respectively.

In Eqs. 13a, 13b, 13c, and 13d, the subscripts of the notations v_0 through v_3 denote the number of pump-pulse-driven switchings of the two potential surfaces. The argument s is omitted in the left-hand-side of Eqs. 13a, 13b, 13c, and 13d. Each function in Eqs. 13a, 13b, 13c, and 13d corresponds to either absorption or stimulated emission from a nonstationary state. As has been pointed out by Pollard et al.;[6] v_0 is the ordinary absorption from $|\phi_0\rangle$, $v_1(\tau)$ is the stimulated emission from $U_{\mathrm{e}}(\tau)|\phi_0\rangle$, $v_2(\tau;\tau_1)$ is the absorption from $U_{\mathrm{g}}(\tau)U_{\mathrm{e}}(\tau_1)|\phi_0\rangle$, and $v_3(\tau;\tau_2,\tau_1)$ is the stimulated emission from $U_{\mathrm{e}}(\tau)U_{\mathrm{g}}(\tau_2)U_{\mathrm{e}}(\tau_1)|\phi_0\rangle$. Notice that every vibrational overlap in Eqs. 13a, 13b, 13c, and 13d with $s=0$ is all unity, so these constituent response functions with $s=0$ convey no vibrational information.

Significance of Grating Arrangement. Now the explanation of our adopting the rather complicated set-up of Fig. 1a is in order. If the material is excited by a train of pulses along just a single arm, the signal has a contribution from the third order polarization as in Eq. 8, which is created by any couple of one of the pump pulses and the probe pulse. From the perturbative point of view the third order polarization yields the dominant feature that is dependent on τ to obscure the faint feature arising from the higher order polarization induced by the multiple excitation. The ordinary transient grating arrangement mitigates this difficulty; if the material is excited by pulse trains on two arms along $\vec{n}_1$ and $\vec{n}_2$, the dominant contribution to the diffraction along $\vec{n}_{\mathrm{p}}\pm2(\vec{n}_1-\vec{n}_2)$ comes from the fifth order polarization and along $\vec{n}_{\mathrm{p}}\pm3(\vec{n}_1-\vec{n}_2)$ from the seventh order polarization, and so forth. By choosing an appropriate direction, therefore, the higher order signal can be detected without being interfered by the lower order signals. However, some difficulty still remains; suppose the case of the double excitation, where a pulse train along $\vec{n}_1$ consists of two pulses ε_1 and ε_3, and the other along $\vec{n}_2$ of ε_2 and ε_4. Then, the fifth order polarization propagating along $\vec{n}_{\mathrm{p}}+2(\vec{n}_1-\vec{n}_2)$ comes from the field products $\varepsilon_{\mathrm{p}}\varepsilon_4^*\varepsilon_3\varepsilon_2^*\varepsilon_1$ ($\varepsilon_{\mathrm{p}}\varepsilon_4\varepsilon_3^*\varepsilon_2\varepsilon_1^*$), $\varepsilon_{\mathrm{p}}\varepsilon_2^*\varepsilon_1\varepsilon_2^*\varepsilon_1$ ($\varepsilon_{\mathrm{p}}\varepsilon_2\varepsilon_1^*\varepsilon_2\varepsilon_1^*$), and $\varepsilon_{\mathrm{p}}\varepsilon_4^*\varepsilon_3\varepsilon_4^*\varepsilon_3$ ($\varepsilon_{\mathrm{p}}\varepsilon_4\varepsilon_3^*\varepsilon_4\varepsilon_3^*$) with the products in the parentheses being for $\vec{n}_{\mathrm{p}}-2(\vec{n}_1-\vec{n}_2)$. The first product leads to the polarization in Eq. 9 with the response function being given by Eq. 11, and the second and the third products also give the polarizations, each being associated with four vibrational terms which are different from the contents of Eq. 11. The set-up in Fig. 1a selectively picks out the polarization given by the first product. As is described later, multiply excited vibrations manifest themselves exclusively through the last component $v_2(\tau;\tau_1)$ in Eq. 11. The relative contribution of this important term is, therefore, reduced from 1/4 to 1/12 by replacing the proposed set-up in Fig. 1a to the set-up with the two excitation arms, say, e.g., along $\vec{n}_1$ and $\vec{n}_2$. In the case of the triple excitation, it is reduced more severely from 1/8 to 1/80. This is why the set-up in Fig. 1a is favored. A similar idea to avoid the interference from the lower order signals has been demonstrated by Bout et al. in their recent Raman echo experiment.[7] As far as the double excitation is concerned, the alternative set-up shown in Fig. 1b is also conceivable, where two

pulses ε_1 along $\vec{n}_1$ and ε_2 along $-\vec{n}_1$ are coincidentally incident on the sample prior to the another coincident pair ε_3 and $\vec{n}_3$ and ε_4 along $-\vec{n}_3$. The dominant contribution to the diffraction along $\vec{n}_p+2(\vec{n}_1-\vec{n}_2)$ is from the fifth order polarization due to the field product of $\varepsilon_p\varepsilon_4\varepsilon_3^*\varepsilon_2^*\varepsilon_1$ ($\varepsilon_p\varepsilon_4^*\varepsilon_3\varepsilon_2\varepsilon_1^*$) for $\vec{n}_p-2(\vec{n}_1-\vec{n}_2)$).

Emphatically, the probe pulse after transmission through the sample should not be detected because the transmitted pulse is unavoidably accompanied by the forward scattering from the third order polarization due to the field products as $\varepsilon_p\varepsilon_1^*\varepsilon_1$, $\varepsilon_p\varepsilon_2^*\varepsilon_2$, and so forth. This is a similar situation to that encountered in the set-up of a single excitation arm.

Detection Scheme. For the sake of simplicity, the optical density effect is neglected. Then the following simple relation holds between the diffracted light $\varepsilon_{ind}(t)$ and its source polarization $\hat{P}(t)$

$$\varepsilon_{ind}(t) = -2\pi ikd\hat{P}(t), \tag{15}$$

where $k\equiv\omega_1/c$, d is the thickness of the sample, and $\hat{P}(t)=\hat{P}^{(i)}(t)$ (i=3, 5, or 7).

In the present study, we adopt a heterodyne detection as shown schematically in Fig. 2, a half mirror designated as BS1 splits a single pulse into two, one being the probe pulse $\varepsilon_p(t)$ and the other its replica $\varepsilon_{lo}(t)$. The temporal separation, say τ, between the last excitation pulses and the probe pulse is varied by VD1 which controls the optical path length before splitting the replica, so the variation of the delay time is transmitted to the replica. The replica $\varepsilon_{lo}(t)$ is not sent into the sample but is mixed with the diffracted light $\varepsilon_{ind}(t)$ by a half-mirror BS2 out of the sample to work as the local oscillator. The delay time of the replica must be adjusted by another controller VD2 so that the replica and the induced field may overlap temporally at the half-mirror BS2 to satisfy $\varepsilon_{lo}(t)=\varepsilon_p(t)$. Once such a coincidence between the two is attained, the controller VD2 is fixed throughout the measurement while VD1 is swept.

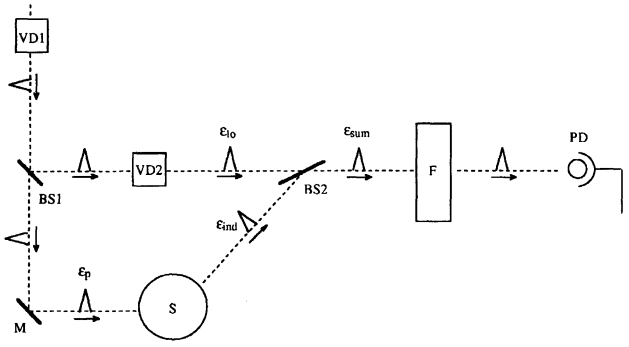

Fig. 2. Schematic representation of the detection scheme: VD1, VD2, controller of optical path length; BS1, BS2, half-mirror; M, mirror; S, sample; F, spectral bandpass filter or monochromator; PD, photodetector. A fine tunability is assumed not for the controller VD1 but for VD2 (see the text).

The sum, $\varepsilon_{sum}(t)=\varepsilon_{lo}(t)+\varepsilon_{ind}(t)$, is received by a square-law detector, and its output is recorded as a function of τ. The τ dependence of the signal is given by the heterodyne product

$$S_{het} = 2\mathscr{Re}\int_{-\infty}^{+\infty} dt\,\{\varepsilon_{lo}^*(t)\varepsilon_{ind}(t)\}. \tag{16}$$

Substituting Eq. 15 with $\hat{P}(t)$ being replaced by Eqs. 7 and 8, or Eq. 9, and $\varepsilon_{lo}(t)$ being expressed explicitly as $\varepsilon_{lo}(t)=\varepsilon_p(t)$, we have

$$S_{het} \sim \mathscr{Re}\{R(0)\},$$

where we use an abbreviated notation $R(s)$ for $R^{(3)}(s, \tau)$, $R^{(5)}(s, \tau, \tau_1)$, or $R^{(7)}(s, \tau, \tau_2, \tau_1)$. Then, as stated above, the beating feature due to the molecular vibration disappears and only a monotonic decay of the electronic origin persists.[3] To avoid the disappearance of the beat, the sum field $\varepsilon_{sum}(t)$ must be dispersed and a spectrally selected component is received by the detector as claimed previously.[3—6] In the dispersed detection, the heterodyne signal $S_{het}(\omega_D)$ is given by[3,5]

$$S_{het}(\omega_D) \sim \mathscr{Re}\int_0^{+\infty} ds e^{-i[(\omega_D-\omega_1)s+\phi]}R(s), \tag{17}$$

where ω_D is a tuned frequency of the monochromator, and ω_1 is a carrier frequency of the probe pulse. The symbol ϕ in Eq. 17 represents the difference between the phases of the local oscillator and of the induced field. In the measurement under consideration, ϕ can take an arbitrary value by finely tuning the delay time of the replica pulse by the controller VD2 within the carrier cycle $2\pi/\omega_1$. Such a fine control can be achieved by a piezoelectric transducer.[8,9] From now on ϕ=0 is assumed as in the ordinary transmission measurement.

The alternative approach to avoid the disappearance of the beat is the homodyne detection as in the ordinary transient grating experiment. The homodyne signal S_{hom} is given by

$$S_{hom} = \int_{-\infty}^{+\infty} dt\,|\varepsilon_{ind}(t)|^2 \sim \int_{-\infty}^{+\infty} dt\,\left|\hat{P}(t)\right|^2 \sim \int_0^{+\infty} ds\,|R(s)|^2.$$

The manifestation of multiply excited vibration is simple and transparent to understand in the heterodyne signal compared with that in the homodyne signal since the former is associated with the response function itself and the latter with its modulus squared. Thus, in the present treatment the heterodyne arrangement including the spectral dispersion is favored over the homodyne arrangement, although the latter would be experimentally much easier than the former.

Now we introduce Fourier transforms $\hat{v}_i$ (i = 0—3) of the constituent response functions v_i in Eqs. 13a, 13b, 13c, and 13d as follows

$$\hat{v}_i \equiv \int_0^{+\infty} \mathrm{d}s e^{-i(\omega_D-\omega_1)s} v_i. \quad (i=0\text{—}3) \tag{18}$$

It is to be noted that each $\hat{v}_i$ represents a frequency spectrum although the frequency dependence as a function of ω_D is not explicitly written out.

With these components Eq. 17 is rewritten as in Eqs. 19, 20, and 21, where the signal $S_{het}(\omega_D)$ is denoted as S_1, S_2, and S_3 for the single, double, and triple excitations, respectively.

$$S_1 \sim e^{-\tau/T_1} \mathscr{Re}\{\hat{v}_0 + \hat{v}_1(\tau)\} \tag{19}$$

$$S_2 \sim -e^{-(\tau+\tau_1)/T_1} \times \mathscr{Re}\{\hat{v}_0 + \hat{v}_1(\tau) + \hat{v}_1(\tau+\tau_1) + \hat{v}_2(\tau;\tau_1)\} \tag{20}$$

$$\begin{aligned} S_3 \sim e^{-(\tau+\tau_2+\tau_1)/T_1} & \times \mathscr{Re}\{\hat{v}_0 + \hat{v}_1(\tau) + \hat{v}_1(\tau+\tau_1) + \hat{v}_1(\tau+\tau_1+\tau_2) \\ & + \hat{v}_2(\tau;\tau_2) + \hat{v}_2(\tau+\tau_2;\tau_1) \\ & + \hat{v}_2(\tau;\tau_2+\tau_1) + \hat{v}_3(\tau;\tau_2,\tau_1)\} \end{aligned} \tag{21}$$

The heterodyne signal has a great advantage over the homodyne in that the signal can be expressed additively. It is to be noted that the signs of S_1 through S_3 differ. The radiation from the $(4n+1)$th order polarization ($n=0, 1, \cdots$) is out of phase to the local oscillator and reduces it as in the ordinary linear absorption while the $(4n+3)$th radiation is in-phase to enhance it.

Results and Discussion

Large Amplitude Vibration. First, we examine some properties of the individual components $\hat{v}_0$ through $\hat{v}_3$ in Eqs. 13a, 13b, 13c, and 13d. Since the motion of the wavepacket given by these equations is quite simple, the following semiclassical interpretation gives a good picture of the optical control of the molecular vibration; suppose a normal mode q with a frequency of ω_v, and suppose that the potential minima are located at $q=0$ in the ground state and at $q=\delta$ in the excited state. By the first switching the initial wavepacket at $q=0$ is vertically transferred to the upper surface, and it begins to move with an amplitude of $\pm\delta$ around $q=\delta$. If the second transfer occurs at the turning point of $q=2\delta$, the wavepacket is forced down to the lower surface with an increased amplitude of $\pm 2\delta$ of motion around the center at $q=0$. The third transfer at the turning point of $q=-2\delta$ brings the wavepacket to the upper surface, and the motion is associated with still a larger amplitude of $\pm 3\delta$ of motion around the center at $q=\delta$. Thus, as shown in Fig. 3, the oscillating amplitude becomes larger by an amount of $\pm\delta$ for each transfer to the other potential surface provided that the repetitive transfers occur with an interval equal to π/ω_v, half a period of the vibrational cycle. To be more rigorous, we may elongate the interval to any multiple of the half period by odd numbers in so far as the vibrational dephasing is insignificant. In the off-resonance case, the corresponding time interval for the repetitive excitation is $2\pi/\omega_v$. This time interval does not lead to any constructive accumulation of the repetitive excitation in the resonant case because two successive transfers with an interval of $2\pi/\omega_v$ act counterbalancingly to leave no gain in the vibrational amplitude.

To reproduce numerically the phased amplification of vibrational motion, we assume a single harmonic mode of frequency $\omega_v=200$ cm^{-1} with a displacement $\delta=1.1$ between the two minima where the displacement δ is defined so as to make the overlap between the two zero-vibrational states as $\exp\{-(1/4)\delta^2\}$. It is also assumed that the vibrational frequency remains the same between the two electronic states. The vibrational overlaps in the integrand of Eqs. 13b, 13c, and 13d are given in Appendix A. The numerical result of $\mathscr{Re}\{\hat{v}_1(\tau)\}$ is shown in Fig. 4a; immediately after the transfer, i.e.,

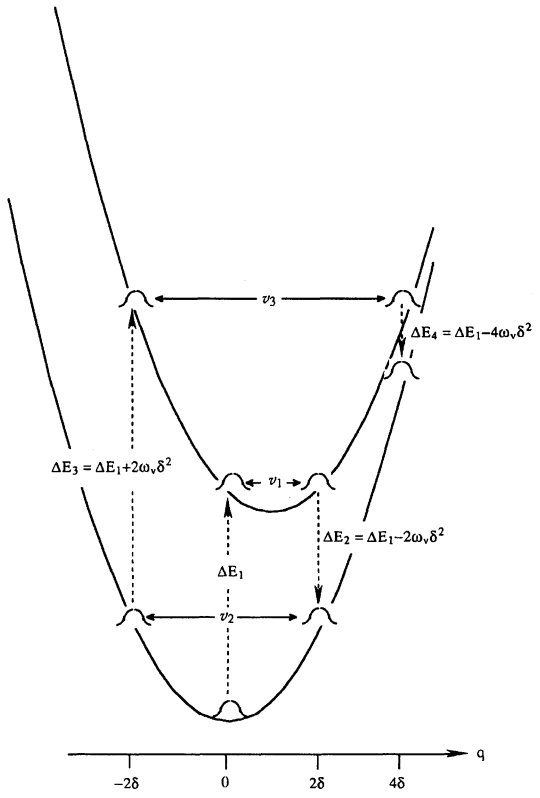

Fig. 3. Schematic representation of the phased amplification of molecular vibration by successive transfers to the counterpart potential surface. The interval of time in the repetitive transfer is one half of the vibrational period. After a transfer, the wavepacket moves with an energy indicated by the horizontal arrows, and its motion until the next transfer can be observed through the annotated element v_i ($i=1$—3). The transition energies between the two states connected by the vertical dashed lines are denoted by ΔE_i ($i=1$—4) according to the semiclassical interpretation, which should correspond to the energies at the peak in the absorption or emission spectrum.

at $\tau=0$ fs, the spectrum, i.e., the frequency dispersion of the signal, is identical to the ordinary absorption spectrum as it should be. It starts to shift to the lower energy side to reach the turning point at $\tau=80$ fs, i.e., π/ω_v, and then goes back to the initial position at $\tau=160$ fs. Such a periodic spectral shift arising from a single transfer has been observed by Fragnito et al.,[4] and the relevant theoretical formulation has been given by Pollard et al.[5,6] When the transfer occurs twice, $v_2(\tau;\tau_1)$ in Eq. 13c is relevant and the spectral behavior of $\mathscr{Re}\{\hat{v}_2(\tau;\tau_1)\}$ is shown in panel (b), where τ_1 is set to be π/ω_v; immediately after the second transfer, i.e., at $\tau=0$ fs, the spectrum is identical to that at $\tau=80$ fs in panel (a). It begins to shift to the higher energy side to reach the turning point at $\tau=80$ fs, and then returns to the initial position at $\tau=160$ fs. This blue-shifted spectrum at $\tau=80$ fs lies in the higher energy region than the spectrum at $\tau=0$ fs in panel (a), which corresponds to the ordinary absorption spectrum. The case of three transfers corresponds to $v_3(\tau;\tau_2,\tau_1)$ in Eq. 13d, and $\mathscr{Re}\{\hat{v}_3(\tau;\tau_2,\tau_1)\}$ is shown in panel (c), where τ_2 as well as τ_1 is set equal to π/ω_v; at $\tau=0$ fs, the spectrum is identical to that at $\tau=80$ fs in panel (b). It starts to shift to the lower energy side to reach the turning point at $\tau=80$ fs, and then returns to the initial position at $\tau=160$ fs in the same way as the two preceding cases. This red-shifted spectrum at $\tau=80$ fs lies in the lower energy region than the spectrum at $\tau=80$ fs in panel (a), or equivalently that at $\tau=0$ fs in panel (b). According to the semiclassical consideration based on the Franck–Condon principle, the energy shift from the center of the ordinary absorption spectrum denoted by ΔE should vary periodically between the two ends $\Delta E=0$ at $\tau=0$ and $\Delta E=-2\omega_v\delta^2$ at $\tau=\pi/\omega_v$ for the case the single transfer, and between $\Delta E=-2\omega_v\delta^2$ at $\tau=0$ and $\Delta E=+2\omega_v\delta^2$ at $\tau=\pi/\omega_v$ for the double transfer, and between $\Delta E=+2\omega_v\delta^2$ at $\tau=0$ and $\Delta E=-4\omega_v\delta^2$ at $\tau=\pi/\omega_v$ for the triple transfer (See Fig. 3). The range of the periodic spectral shift, therefore, should be increased by an amount of $2\omega_v\delta^2$ for each single transfer. Such a semiclassical predictions are in good agreement with the features depicted in Fig. 4.

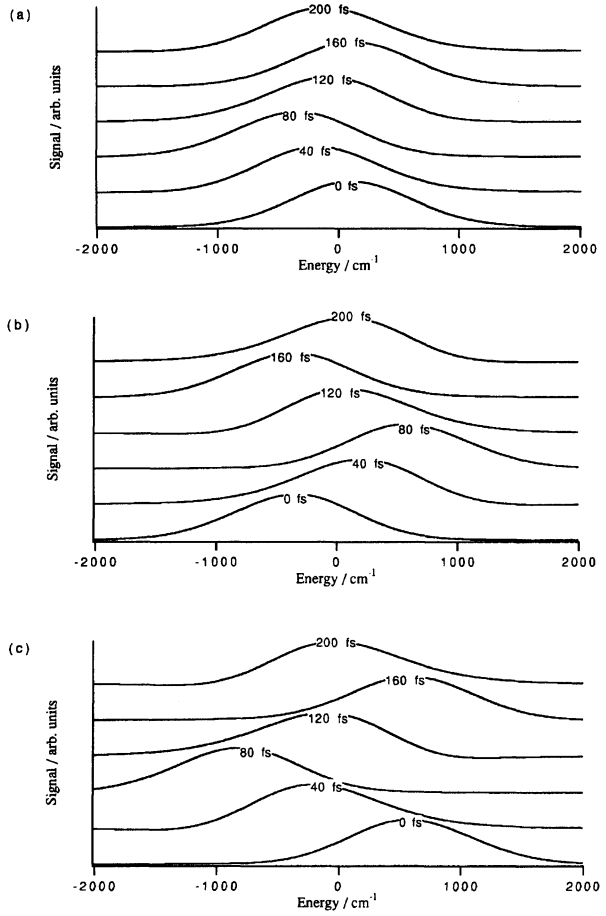

Fig. 4. Numerical results of $\mathscr{Re}\{\hat{v}_1(\tau)\}$ (a), $\mathscr{Re}\{\hat{v}_2(\tau;\tau_1)\}$ (b), and $\mathscr{Re}\{\hat{v}_3(\tau;\tau_2,\tau_1)\}$ (c) calculated for several values of the parameter τ. The abscissas are taken for $\omega_D-\omega_0$, where ω_D is a tuned frequency of the monochromator and ω_0 is the purely electronic transition frequency. Furthermore, the carrier frequency of optical pulses is assumed to be identical to the purely electronic transition frequency, that is, $\omega_1-\omega_0=0$. In the calculation we have used parameters of $T_2=120$ fs and $\sigma=320$ cm^{-1}.

As shown in Eqs. 19, 20, and 21, the observed signal consists a number of components, one of which is the contribution from the vibrational motion prepared by the most frequent excitations, and the rest are the contributions from the vibrations created by less frequent excitations. In so far as $\tau_1=\tau_2=\pi/\omega_v$, the individual components of $\mathscr{Re}\{\hat{v}_0\}$ through $\mathscr{Re}\{\hat{v}_3(\tau;\tau_2,\tau_1)\}$ behave differently from the others, particularly in the region of energy where each spectrum moves about. This feature makes it possible to identify the most important contribution, that is, $\mathscr{Re}\{\hat{v}_1(\tau)\}$ in S_1, $\mathscr{Re}\{\hat{v}_2(\tau;\tau_1)\}$ in S_2, or $\mathscr{Re}\{\hat{v}_3(\tau;\tau_2,\tau_1)\}$ in S_3. Figure 5 shows the observed signals S_1 through S_3as τ is varied; the detected frequency is tuned lower in panel (a), and higher in (b) by 1200 cm^{-1} than the zero–zero transition frequency in the ordinary absorption spectrum; in the double excitation, the component from the double transfer, $\mathscr{Re}\{\hat{v}_2(\tau;\tau_1)\}$, is more prominent in (b) than in (a), whereas in the triple excitation, the component from the triple transfer, $\mathscr{Re}\{\hat{v}_3(\tau;\tau_2,\tau_1)\}$, is more dominant in (a) than in (b). Thus, one can selectively detect the highly excited vibration as the primary feature by monitoring it through the frequency far from the center of the absorption spectrum. As is evident from Fig. 5, the effective direction of detuning depends on the excitation mode; the red-shift is favored for the triple excitation whereas the blue-shift for the double excitation.

Mode Selective Excitation. So far, it is assumed that the material has only one active vibrational mode. Under the influence of a definite number of excitation pulses, selective excitation in the general multimode system is prohibited by the fact that the vibra-

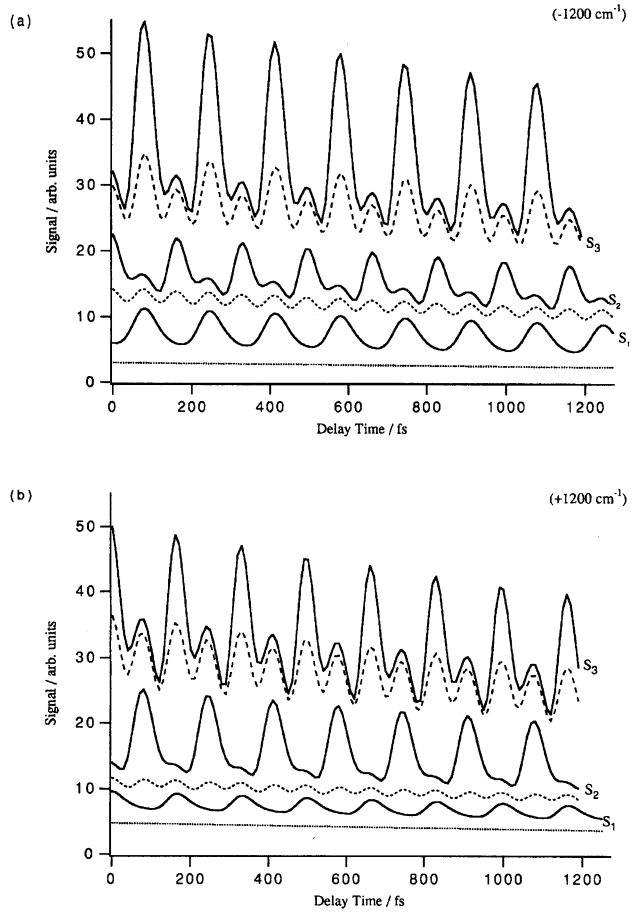

Fig. 5. Numerical results of S_1 through S_3 (solid lines with the annotations) as a function of τ. Although S_2 in Eq. 20 accompanies a negative sign, it is ignored in the figure. The detuning frequency $\omega_D - \omega_0$ is fixed to -1200 cm^{-1} in (a) and $+1200$ cm^{-1} in (b). The densely dotted, fine dashed, and coarse dashed lines show $S_1 - e^{-\tau/T_1}\mathcal{R}e\{\hat{v}_1(\tau)\}$, $S_2 - e^{-(\tau+\tau_1)/T_1}\mathcal{R}e\{\hat{v}(\tau; \tau_1)\}$ and $S_3 - e^{-(\tau+\tau_2+\tau_1)/T_1}\mathcal{R}e\{\hat{v}_3(\tau; \tau_2, \tau_1)\}$, respectively. They indicate background levels from contributions other than the most important ones. Meaningful comparison of intensity is possible only among a set of four traces, i.e., a solid line in (a), its background and their counterparts in (b). In the calculation we have assumed $T_1 = 4.8$ ps.

tional motion can no longer be recursive unless all the ratios of two frequencies involved are rational numbers. Here we confine ourselves into a simple system of two vibrational modes and assume that the two frequencies are well separated from each other. Our purpose is to see the effect of the selective excitation of the vibrational mode of a low frequency ω_L in the presence of another vibrational mode of a high frequency ω_H. By virtue of Assumption 4 we can discuss such a system meaningfully. Note that the pump-probe method is suited for the observation of such a low frequency vibrational mode that is buried under the linewidth due to a T_2 process, while the photon echo method is not appropriate for the detection of such a low frequency vibration because the echo polarization decays within the characteristic time constant T_2.

As mentioned above, a sequence of interactions results in the effective amplification of vibration if the temporal separation is equal to the multiples by odd numbers of the half period of the vibrational cycle, while the multiples by even numbers are ineffective. This is a key point to achieve the selective enhancement of a lower frequency mode. To be more general, if the following relation holds for the two frequencies

$$\omega_L/\omega_H = (2n-1)(2m), \quad (m \text{ and } n = 1, 2, \cdots) \tag{21}$$

the interpulse separation equal to $(2n-1)\pi/\omega_L = 2m\pi/\omega_H$ promises the selective excitation successfully. However, in a real experiment, n in the numerator should be as small as possible not to suffer from the vibrational dephasing.

The numerical results are shown in Fig. 6, where we assume frequencies of $\omega_L = 200$ and $\omega_H = 1600$ cm^{-1} fulfilling the relation in Eq. 21. Panels (a)—(c) correspond to the single, double, and triple excitation cases, respectively. The dashed lines are for the single vibrational mode without the high frequency vibration. Comparison of the dashed curves in (a)—(c) reveals that the oscillational feature of the curves increases from the single toward triple excitation, while no significant change is seen for the higher frequency oscillation.

The author (H. K.) was financially supported by JSPS Fellowships for Japanese Junior Scientists.

Appendix A. Vibrational Overlaps in Eqs. 13b, 13c, and 13d.

Referring to Ref. 10, one can evaluate the vibrational overlaps in Eqs. 13b, 13c, and 13d. The motion of a Gaussian wavepacket on a harmonic surface is obtained with a particular ease. From the calculation, all the vibrational responses in Eqs. 13b, 13c, and 13d can be written in the common form

$$\exp\left[-(1/2)\delta^2\left\{(1/2)\left(f_1{}^2 + f_2{}^2\right) + i\,(f_2 f_3 - f_4)\right\}\right]. \tag{A1}$$

The results for the three cases are summarized as follows.

For $\langle\phi_0|\,U_e^\dagger(\tau+s)\,U_g(s)\,U_e(\tau)|\phi_0\rangle$ in Eq. 13b,

$$f_1 = \sin\ \theta,\ f_2 = 1 - \cos\theta,\ f_3 = -2\sin(\varphi+\theta) + \sin\theta,$$

and

$$f_4 = \sin(\varphi + 2\theta) - \sin\varphi - \sin\theta\cos\theta, \tag{A2}$$

where $\varphi = \omega_v\tau$ and $\theta = \omega_v s$.

For $\langle\phi_0|\,U_e^\dagger(\tau_1)\,U_g^\dagger(\tau)\,U_e^\dagger(s)\,U_g(s+\tau)\,U_e(\tau_1)|\phi_0\rangle$ in Eq. 13c,

$$f_1 = \sin\theta,\ f_2 = 1 - \cos\theta,$$
$$f_3 = -2\sin(\varphi_1 + \varphi + \theta) + 2\sin(\varphi+\theta) - \sin\theta,$$

and

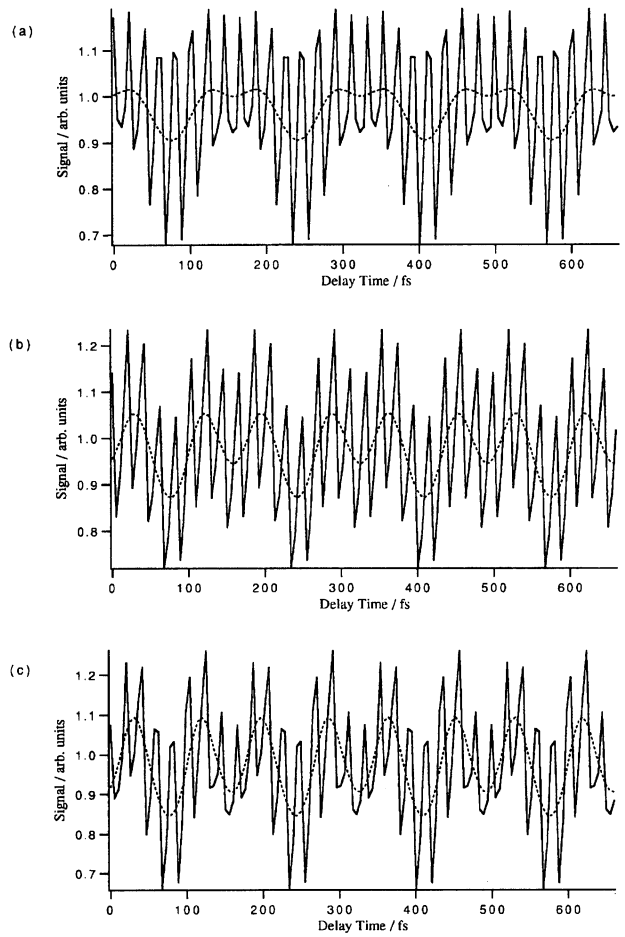

Fig. 6. Numerical results of S_1 through S_3 for a system having two active modes, one with a frequency of ω_L=200 cm^{-1} and the other with ω_H=1600 cm^{-1}. Panels (a)—(c) correspond to the single, double, and triple excitation cases, respectively. The dashed lines show results for the system of a single mode without the higher frequency mode. All the traces are normalized so as to give the same area under the traces. In the calculation, we have used the parameters of δ (200 cm^{-1})=1.1, δ (1600 cm^{-1})=1.0, T_2=120 fs, σ=320 cm^{-1}, and $\omega_D=\omega_1=\omega_0$. The decay of the electronic population inversion is assumed to be slow enough to regard T_1 as being infinite.

$$f_4 = \sin(\varphi_1+\varphi+2\theta) - \sin(\varphi+2\theta) - \sin(\varphi+\theta) + \sin\varphi + \sin\theta\cos\theta, \quad \text{(A3)}$$

where $\varphi_1=\omega_v\tau_1$, $\varphi=\omega_v\tau$ and $\theta=\omega_v s$.

For $\langle\phi_0|U_e^\dagger(\tau_1)U_g^\dagger(\tau_2)U_e^\dagger(\tau+s)U_g(s)U_e(\tau)U_g(\tau_2)U_e(\tau_1)|\phi_0\rangle$ in Eq. 13d,

$$f_1 = \sin\theta,\ f_2 = 1-\cos\theta,$$
$$f_3 = -2\sin(\varphi_1+\varphi_2+\varphi+\theta) + 2\sin(\varphi_2+\varphi+\theta) - 2\sin(\varphi+\theta) + \sin\theta,$$

and

$$f_4 = \sin(\varphi_1+\varphi_2+\varphi+2\theta) - \sin(\varphi_1+\varphi_2+\varphi) - \sin(\varphi_2+\varphi+2\theta) + \sin(\varphi_2+\varphi) + \sin(\varphi+2\theta) - \sin\varphi - \sin\theta\cos\theta, \quad \text{(A4)}$$

where $\varphi_1=\omega_v\tau_1$, $\varphi_2=\omega_v\tau_2$, $\varphi=\omega_v\tau$, and $\theta=\omega_v s$.

Appendix B. Grating Experiment with Intense Optical Pulses.

Here, some comments will be made on the grating experiment employing so intense optical puses as to require nonperturbative approach in solving the Liouville equation

$$\dot\rho(t) = -i[\mathscr{H}_0 + \mathscr{H}_1, \rho(t)]. \quad \text{(B1)}$$

The field free Hamiltonian $\mathscr{H}_0$ is given by

$$\mathscr{H}_0 = |g\rangle H_g\langle g| + |e\rangle(\omega_0 + H_e)\langle e|, \quad \text{(B2)}$$

where the electronic ground and excited states are denoted as $|g\rangle$ and $|e\rangle$, respectively. The vibrational Hamiltonians in the two electronic states are denoted as H_g and H_e. The symbol ω_0 stands for the frequency of the purely electronic transition between the two. The optical interaction $\mathscr{H}_1$ is described by

$$\mathscr{H}_1 = -p_{ge}\sigma_x E(t,\vec r). \quad \text{(B3)}$$

where p_{ge} represents the transition dipole moment, σ_x denotes the x component of the Pauli operators in the form of $\sigma_x\equiv|g\rangle\langle e|+|e\rangle\langle g|$. Corresponding notations for y and z components are reserved for later use. The case of the triple excitation is taken representatively. In this case the sample is irradiated by three pairs of excitation pulses at $t=t_1$, t_2, and t_3, and a probe pulse is incident at the moment of $t=t_p$. Then the externally applied field $E(t,\vec r)$ can be written as

$$E(t,\vec r) = \varepsilon(t,\vec r)\,e^{i\omega t} + \text{c.c.}$$
$$\varepsilon(t,\vec r) = \varepsilon_1[\exp\{-i(\omega/c)(\vec n_1\cdot\vec r)\} + \exp\{-i(\omega/c)(\vec n_2\cdot\vec r)\}] \text{ for } t_1^- < t < t_1^+, \quad \text{(B4)}$$
$$= \varepsilon_2[\exp\{-i(\omega/c)(\vec n_3\cdot\vec r)\} + \exp\{-i(\omega/c)(\vec n_4\cdot\vec r)\}] \text{ for } t_2^- < t < t_2^+,$$
$$= \varepsilon_3[\exp\{-i(\omega/c)(\vec n_5\cdot\vec r)\} + \exp\{-i(\omega/c)(\vec n_6\cdot\vec r)\}] \text{ for } t_3^- < t < t_3^+,$$
$$= \varepsilon_p\exp\{-i(\omega/c)(\vec n_p\cdot\vec r)\} \text{ for } t_p^- < t < t_p^+, \quad \text{(B5)}$$

where t_i^- and t_i^+ (i=1—3 and p) indicate the moments just before and after t_i, respectively. Then we introduce a density operator $\hat\rho(t)$ on a rotating frame defined by

$$\hat\rho(t) \equiv V_1\rho(t)V_1^\dagger \text{ with}$$
$$V_1 \equiv \exp[-(i/2)\sigma_z\{\omega t - (1/2)(\phi_1+\phi_2)\}], \quad \text{(B6)}$$

where $\phi_i\equiv(\omega/c)(\vec n_i\cdot\vec r)$ (i=1—6 and p).
During the first optical irradiation, the equation for $\hat\rho(t)$ takes the from

$$\dot{\hat\rho}(t) = -i\left[-(\Delta/2)\sigma_z + (1/2)\left(\hat 1+\sigma_z\right)H_g + (1/2)\left(\hat 1-\sigma_z\right)H_e - 2p_{ge}\varepsilon_1\cos(\phi_{21}/2)\sigma_x, \hat\rho(t)\right], \quad \text{(B7)}$$

where $\hat{1}$ signifies a unit operator for the electronically two-level system, $\Delta \equiv \omega_0 - \omega$, and $\phi_{ij} \equiv \phi_i - \phi_j$. In this period, the material system can be treated as being driven only by the external field because the Rabi frequency is assumed to be sufficiently large. Then $\hat{\rho}(t)$ obeys the equation

$$\dot{\hat{\rho}}(t) = -i\left[-2p_{ge}\varepsilon_1 \cos\left(\phi_{21}/2\right)\sigma_x, \hat{\rho}(t)\right]. \tag{B8}$$

From Eq. 8, we have

$$\hat{\rho}\left(t_1^+\right) = \mathscr{L}_x\left(\theta_1\right)\hat{\rho}\left(t_1^-\right), \tag{B9}$$

where $\theta_1 \equiv 4p_{ge}\varepsilon_1\{\cos\left(\phi_{21}/2\right)\}\left(t_1^+ - t_1^-\right)$ and $\mathscr{L}_x(\theta)$ is defined by

$$\mathscr{L}_i(\theta)\hat{O} \equiv \exp\left\{(i/2)\sigma_i\theta\right\}\hat{O}\ \exp\left\{-(i/2)\sigma_i\theta\right\}. \quad (i = x, y, \text{ or } z) \tag{B10}$$

Until the next irradiation, the system is under influence of the field free terms in Eq. B7 and evolves into $\hat{\rho}(t_2^-)$ given by

$$\hat{\rho}\left(t_2^-\right) = \mathscr{L}_z\left(\Delta\left(t_2^- - t_1^+\right)\right)\mathscr{L}_0\left(t_2^- - t_1^+\right)\hat{\rho}\left(t_1^+\right), \tag{B11}$$

where

$$\mathscr{L}_0(\tau)\hat{O} \equiv \exp\left\{-i\left(P_gH_g + P_eH_e\right)\right\}\hat{O} \times \exp\left\{i\left(P_gH_g + P_eH_e\right)\right\}. \tag{B12}$$

In Eq. B12, we introduce projection operators defined by $P_i \equiv |i\rangle\langle i|$ ($i = g$ and e). Repeating a similar procedure, we find the time development of the material state for $t \geq \tau + \tau_2 + \tau_1$

$$\begin{aligned}\hat{\rho}(t) = {} & \left\{\mathscr{L}_z\left(\Delta\left(t-\tau-\tau_2-\tau_1\right)\right)\mathscr{L}_0\left(t-\tau-\tau_2-\tau_1\right)\right\} \\ & \times\left\{\mathscr{L}_x\left(\theta_p\right)\mathscr{L}_z\left(\phi_{p56}\right)\right\} \\ & \times\left\{\mathscr{L}_z(\Delta\tau)\mathscr{L}_0(\tau)\right\}\left\{\mathscr{L}_x\left(\theta_3\right)\mathscr{L}_z\left(\phi_{5634}\right)\right\} \\ & \times\left\{\mathscr{L}_z\left(\Delta\tau_2\right)\mathscr{L}_0\left(\tau_2\right)\right\}\left\{\mathscr{L}_x\left(\theta_2\right)\mathscr{L}_z\left(\phi_{3412}\right)\right\} \\ & \times\left\{\mathscr{L}_z\left(\Delta\tau_1\right)\mathscr{L}_0\left(\tau_1\right)\right\}\mathscr{L}_x\left(\theta_1\right)\hat{\rho}(0),\end{aligned} \tag{B13}$$

where $\theta_2 \equiv 4p_{ge}\varepsilon_2\{\cos\left(\phi_{43}/2\right)\}\left(t_2^+ - t_2^-\right)$, $\theta_3 \equiv 4p_{ge}\varepsilon_3\{\cos\left(\phi_{65}/2\right)\}\left(t_3^+ - t_3^-\right)$, $\theta_p \equiv 2p_{ge}\varepsilon_p\left(t_p^+ - t_p^-\right)$, $\phi_{ijkl} \equiv (1/2)(\phi_i + \phi_j) - (1/2)(\phi_k + \phi_l)$, and $\phi_{ijk} \equiv \phi_i - (1/2)(\phi_j + \phi_k)$. In deriving Eq. B13, we have set $t_1^- \approx t_1 = 0$, $t_2^- - t_1^+ \approx t_2 - t_1 = \tau_1$, $t_3^- - t_2^+ \approx t_3 - t_2 = \tau_2$, $t_p^- - t_2^+ \approx t_p - t_2 = \tau$, and $t_p^+ \approx t_p = \tau + \tau_2 + \tau_1$ since an optical irradiation is instantaneous on the time scale of the investigated dynamics. The initial condition is given by

$$\hat{\rho}(0) = (1/2)\left(\hat{1} + \sigma_z\right) \otimes \{|\phi_0\rangle\langle\phi_0|\} \tag{B14}$$

with $|\phi_0\rangle$ designating the zero vibrational state in the electronic ground state. Note that Assumption 4 in the text saves labor greatly in the calculation of Eq. B13 because the electronic coherence decays out completely within an interval between the neighboring irradiations.

The material polarization can be expressed as

$$P(t) = \hat{P}(t)\ \exp\left\{i\left(\omega t - \phi_p\right)\right\} + \text{c.c.}. \tag{B15}$$

The temporal envelope $\hat{P}(t)$ is defined by

$$\hat{P}(t) \equiv \mathscr{N} p_{ge} tr\left(\hat{\rho}(t)\sigma^+\right) \text{ with } \sigma^+ \equiv (1/2)\left(\sigma_x - i\sigma_y\right), \tag{B16}$$

where $\mathscr{N}$ signifies the number density of the absorbers. Combining the result of Eq. B13 with Eq. B16, we find the envelope for $s \geq 0$

$$\begin{aligned}\hat{P}\left(s+\tau+\tau_2+\tau_1\right) \propto {} & -i\sin\theta_p \\ & \times\{(1+\cos\theta_3)(1+\cos\theta_2)(1+\cos\theta_1)v_0 \\ & +(-1+\cos\theta_3)(1+\cos\theta_2)(1+\cos\theta_1)v_1(\tau) \\ & +(1+\cos\theta_3)(-1+\cos\theta_2)(1+\cos\theta_1)v_1(\tau+\tau_2) \\ & +(1+\cos\theta_3)(1+\cos\theta_2)(-1+\cos\theta_1) \\ & \times v_1(\tau+\tau_2+\tau_1) \\ & +(1+\cos\theta_3)(-1+\cos\theta_2)(-1+\cos\theta_1) \\ & \times v_2(\tau+\tau_2;\tau_1) \\ & +(-1+\cos\theta_3)(-1+\cos\theta_2)(1+\cos\theta_1)v_2(\tau;\tau_2) \\ & +(-1+\cos\theta_3)(1+\cos\theta_2)(-1+\cos\theta_1) \\ & \times v_2(\tau;\tau_2+\tau_1) \\ & +(-1+\cos\theta_3)(-1+\cos\theta_2)(-1+\cos\theta_1) \\ & \times v_3(\tau;\tau_2,\tau_1)\}.\end{aligned} \tag{B17}$$

The factor $\cos\theta_i$ in Eq. B17 can be expanded into $1 - (1/2!)\theta_i^2 + (1/4!)\theta_i^4 - \cdots$. The pulse areas θ_i ($i = 1$—3) have a spatial dependence according to their definitions. Then the product $\theta_3^2\theta_2^2\theta_1^2$ includes the factor $\exp\{i(\pm\phi_{65}\pm\phi_{43}\pm\phi_{21})\}$. This is combined with the phase factor in Eq. B15 to yield

$$\begin{aligned}&\exp\left[i\left\{\omega t - \left(\phi_p \pm \phi_{65} \pm \phi_{43} \pm \phi_{21}\right)\right\}\right] \\ &\quad = \exp\left[i\omega\left\{t - (1/c)\right.\right. \\ &\qquad \left.\left.\times\left(\vec{n}_p \pm \Delta\vec{n}_{65} \pm \Delta\vec{n}_{43} \pm \Delta\vec{n}_{21}\right)\cdot\vec{r}\right\}\right],\end{aligned} \tag{B18}$$

with $\Delta\vec{n}_{ij} \equiv \vec{n}_i - \vec{n}_j$. The spatial dependence in Eq. B18 accounts for the diffraction into the direction of $\vec{n}_p \pm \Delta\vec{n}_{65} \pm \Delta\vec{n}_{43} \pm \Delta\vec{n}_{21}$. Collecting all terms in Eq. B17 proportional to $\exp\{i(\pm\phi_{65}\pm\phi_{43}\pm\phi_{21})\}$, it is found that the diffraction under intense pulses gives the signal consisting of the equivalent eight components which are all the same except for the absolute intensity as that from weak pulses discussed in the text.

References

1) A. M. Weiner, D. E. Leaird, G. P. Wiederrecht, and K. A. Nelson, *Science*, **247**, 1317 (1990).
2) J. J. Gerdy, M. Dantus, R. M. Bowman, and A. H. Zewail, *Chem. Phys. Lett.*, **171**, 1 (1990).
3) H. Kawashima and T. Shida, *J. Chem. Phys.*, **98**, 4446 (1993).
4) H. L. Fragnito, J. Y. Bigot, P. C. Becker, and C. V. Shank, *Chem. Phys. Lett.*, **160**, 101 (1989).
5) W. T. Pollard, H. L. Fragnito, J. Y. Bigot, C. V. Shank, and R. A. Mathies, *Chem. Phys. Lett.*, **168**, 239 (1990).
6) W. T. Pollard, S. Y. Lee, and R. A. Mathies, *J. Chem. Phys.*, **92**, 4012 (1990).
7) D. V. Bout, L. J. Muller, and M. Berg, *Phys. Rev. Lett.*, **67**, 3700 (1991).

8) N. F. Scherer, R. J. Carlson, A. Matro, M. Du, A. J. Ruggiero, V. Romero-Rochin, J. A. Cina, G. R. Fleming, and S. A. Rice, *J. Chem. Phys.*, **95**, 1487 (1991).
9) N. F. Scherer, A. Matro, L. D. Ziegler, M. Du, R. J. Carlson, J. A. Cina, and G. R. Fleming, *J. Chem. Phys.*, **96**, 4180 (1992).
10) E. J. Heller, *J. Chem. Phys.*, **62**, 1544 (1975).